Brune, S., Williams, S. E., Butterworth, N. P., Müller, R. D. (2016): Abrupt plate accelerations shape rifted continental margins. - Nature, 536, 7615, 201-204.

https://doi.org/10.1038/nature18319

Abrupt plate accelerations shape rifted continental margins

Sascha Brune[1,2], Simon E. Williams[2], Nathaniel P. Butterworth[2], and R. Dietmar Müller[2]

[1] GFZ German Research Centre for Geosciences, Potsdam, Germany
[2] EarthByte Research Group, School of Geosciences, University of Sydney, Australia

Rifted margins are formed by persistent stretching of continental lithosphere until break-up is achieved. It is well known that strain-rate dependent processes control rift evolution[1,2], yet quantified extension histories of Earth's major passive margins have become available only recently. We investigate rift kinematics globally by applying a new geotectonic analysis technique to revised global plate reconstructions. We find that rifted margins feature an initial, slow rift phase (< 10 mm/yr, full rate) and that abrupt acceleration of plate divergence introduces a fast rift phase. Plate acceleration takes place before continental rupture and significant margin area is created during each phase. We reproduce the rapid transition from slow to fast extension using analytical and numerical modelling with constant-force boundary conditions. The extension models suggest that the two-phase velocity behaviour is caused by a rift-intrinsic strength-velocity feedback, which can be robustly inferred for diverse lithosphere configurations and rheologies. Our results explain differences between proximal and distal margin areas[3] and demonstrate that abrupt plate acceleration during continental rifting is controlled by the nonlinear decay of the resistive rift strength force. This mechanism presents a new explanation for several previously unexplained rapid absolute plate motion changes providing new insights into the balance of plate driving forces through time.

Rifted continental margins, with an overall length of more than 100,000 km, are the longest tectonic features on our planet, two times longer than spreading ridges or convergent plate boundaries. During formation of rifted margins, new continental surface area is generated by normal faulting and volcanic intrusions. Both processes are dependent on extension velocity, which governs the thermal configuration of the rift and hence the depth of the brittle-ductile transition and the length of normal faults[1], as well as the degree of decompression melting and serpentinisation[4]. Moreover, rift velocity has been shown to control rift symmetry and the formation of hyper-extended crust[5].

Quantifying the history of extension velocity at rifted margins requires knowledge of the motions between diverging plates and of the timing of continental break-up. Recently, revised regional syn-rift plate models for the opening of the Atlantic, South China Sea, Gulf of California and Australia-Antarctica rifting have become available (see Supplementary Table 1). Here, we incorporate these regional studies in a global plate kinematic model[6] and use an updated, simplified global set of boundaries between continental and oceanic crust (COBs) in order to explore continental break-up processes. We exploit the fact that in a pre-rift reconstruction, present-day COBs from

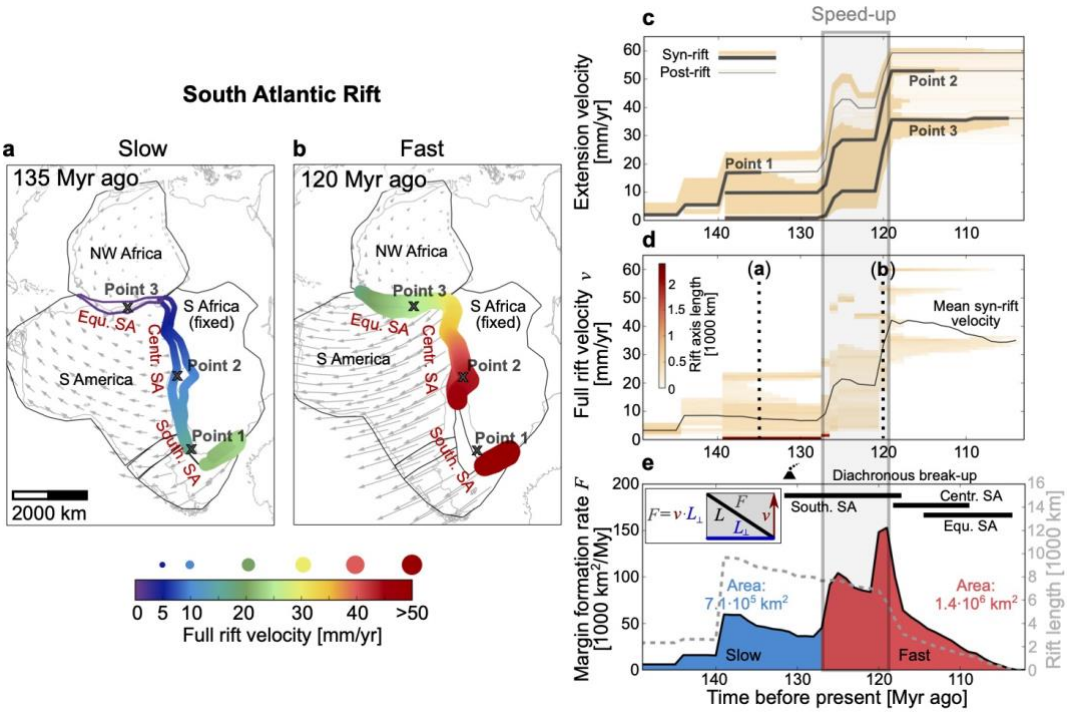

Figure 1 | Rift velocity evolution of the South Atlantic.
(a,b) *Rift velocities (coloured circles) are evaluated at overlapping plate polygons (black) with rift-ward polygon boundaries being defined through present day COBs.* ***(c)*** *Extension velocity evolution of all rift points showing the syn-rift and post-rift phase (thick and thin lines, respectively).* ***(d)*** *Frequency of syn-rift velocities in terms of rift axis length. Colours display the integrated length of all rift segments deforming at the same velocity. The black line shows mean velocity of all syn-rift segments. The fast rift phase starts ~126 Myr ago.* ***(e)*** *The margin formation rate F at each rift segment of length L is computed by multiplying rift velocity v and velocity-orthogonal length of the segment $L_\perp$. Total rift length is shown as grey dashed line. Timing of Paraná-Etendeka flood basalts is depicted by volcano symbol. Black horizontal bars indicate diachronous break-up. An animation of the kinematic evolution can be found in the supplement.*

conjugate passive margins will show significant overlap, since the plate tectonic models do not explicitly incorporate lithospheric deformation. As the plates move apart the overlap decreases, and the time when conjugate COBs disconnect defines break-up, the transition from rifting to seafloor spreading (Fig. 1).

We extract the local rift velocity via pyGPlates, a novel Python library that allows script-based access to the plate reconstruction software GPlates. We subdivide each COB in segments of ~50 km length, and compute the relative velocity between the two contributing plates at each segment (Fig. 1c). First we address the question: Is there a systematic trend in the temporal evolution of extension velocity within entire rift systems? We visualise the velocity evolution of the rift system in a single diagram by displaying the integrated rift axis length of all segments that deform within a certain velocity range in 1 Myr time intervals (Fig. 1d). We discard any segment where break-up is accomplished, i.e. where COBs don't overlap anymore. Hence, the analysed plate boundary length declines through time (see dashed grey line in Fig. 1e) and reduces to zero at final plate separation. We explicitly exclude failed rifts from our analysis, because they do not contribute to passive margin formation.

In addition to rift velocity we compute the rate of rifted margin formation, i.e. the product of the extension velocity and the velocity-orthogonal length of each COB segment. Integration along both conjugate margins and division by 2 yields the overall rate of rifted margin formation F. The formation rate F increases with extension velocity and decreases when individual segments are discarded during diachronous break-up (Fig. 1e). Note that F is independent of the distance between hinge line and COB, instead representing the newly created margin surface. This allows us to draw robust conclusions on rifted margin growth as no assumptions about previous rift phases, or initial crustal and lithospheric thickness have to be made.

With a rift length of more than 10,000 km, the South Atlantic Rift (Fig. 1) generated 2.1x10^6 km^2 of rifted margin area, more than any other Phanerozoic continental rift. During the first 25 Myr of extension, the Euler pole is located close to the equatorial Atlantic Rift[7,8]; therefore rifting is faster in the South. The mean rift velocity remains relatively low (< 10 mm/yr, full rate) until it increases rapidly to more than 35 mm/yr within 6 Myr. This speed-up at ~126-120 Myr ago coincides with severe loss of strength in the equatorial Atlantic Rift[9] suggesting rift weakening as a controlling parameter. Both rift phases shape the rifted margins: about one third of the South Atlantic margin area was formed during the slow, and two third during the fast phase (Fig. 1e).

This two-phase velocity history is a common feature of many other rift systems, illustrated for the central North Atlantic, North America - Iberia, Australia - Antarctica and South China Sea rifting in Fig. 2 and for the Gulf of California, the North East Atlantic and North America - Greenland in Extended Data Figures 3 and 4. Consistently, the fast rift phase starts ~10 Myr before inception of break-up and persists until plate separation is complete. Both the slow and the fast phase contribute significantly to shaping the rifted margins. All regional tectonic reconstructions used here, compiled from a range of independent studies, result in the same two-phase pattern, underlining the robustness of our results. Moreover, using alternative reconstructions for the South Atlantic does not change our conclusions (Extended Data Fig. 8).

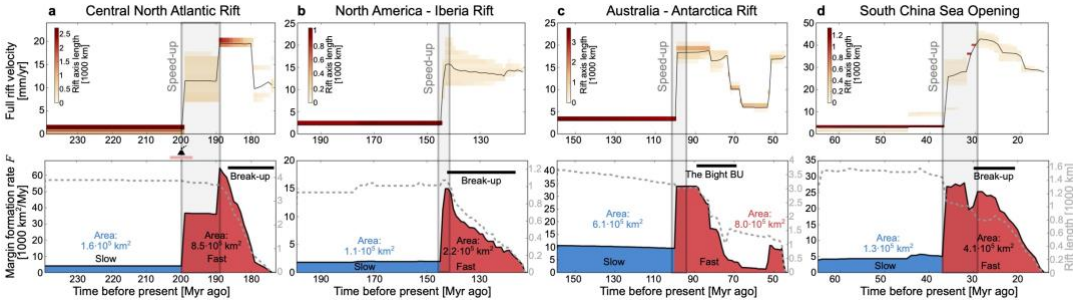

Figure 2 | Other rift systems

All depicted rifts exhibit a two-phase velocity history. A rapid plate acceleration precedes inception of break-up by ~10 Myr. Timing of CAMP flood basalts is depicted by volcano symbol in (a). Corresponding map views are shown in Extended Data Fig. 1-3. An animation of the kinematic evolution of each rift can be found in the supplement.

We conduct robustness tests for all case studies using alternative COBs defined by the extreme landward limit of basement that is not clearly continental crust. These COB polygons are located closer to the coastline, which shortens the duration of rifting by several million years. Nevertheless, the contributions of both phases in shaping the rifted margins remain significant (Extended Data Figures 5,6).

In order to evaluate the geodynamic response of a rift zone to plate driving forces, we use 2D analytical and numerical models. While the most common modelling approach is to prescribe a constant velocity at the model boundary[5,10], here we use a force boundary condition[11–13] allowing for self-consistent computation of velocity evolution. The force boundary condition is applicable to major rifts where the integrated strength of the entire rift system is comparable to the plate driving forces, such as those considered here.

First, we develop an analytical model of a homogeneous lithospheric layer that deforms according to power law rheology under a constant force. For simplicity, we neglect depth-dependent thinning, non-constant temperature and compressibility; however these processes are incorporated within the numerical models below. The resulting velocity equals $L/(n\ t_r) \cdot (1-t/t_r)^{-1}$, where L is the width of the necking zone, n the dislocation creep stress-exponent, t_r the duration of rifting and t is time (see Methods for derivation). The formula is plotted in Fig. 3c using typical parameter values of L=100 km and t_r=20 Myr. Realistic values[14] for n range between 3 and 4, hence we approximate a purely viscous lithosphere by n=3.5 (Model A1). Introducing brittle failure as a highly non-linear end-member of power law creep[12] we also show solutions for n=10 (Model A2) and n=30 (Model A3). In all cases, rifting commences slowly, yet velocities increase within a few million years, where the short duration of speed-up is caused by the power law rheology of the lithosphere.

Numerical modelling accounts for more realistic evolution of deformation, temperature, and buoyancy, but the resulting velocity evolution is very similar to the analytical solution (Fig. 3c). The reason for the acceleration is a feed-back mechanism that we term dynamic rift weakening: as long as the rift is strong, extension rate is low (Fig. 3a), but with continued deformation the rift centre becomes successively weaker due to necking and strain softening (Fig. 3b). Loss of strength accelerates rifting, which results in new strength loss and causes conjugate rift sides to accelerate rapidly[15,16]. We show 10 models with varying rheological flow laws, thermal configurations, layer thicknesses, frictional softening, and thermal expansivity (Fig. 3 and Extended Data Fig. 7). The two-phase behaviour and the abruptness of speed-up are robustly represented by any of these models. The numerical experiments also demonstrate that a variation of the extensional tectonic forces applied at the model boundaries affects the duration of the first, slow rift phase. Increasing the boundary force leads to earlier rift acceleration and breakup, while reducing the force prolongs the slow rift phase, or even generates a failed rift where conductive cooling and thermal strengthening decrease the extension rate until

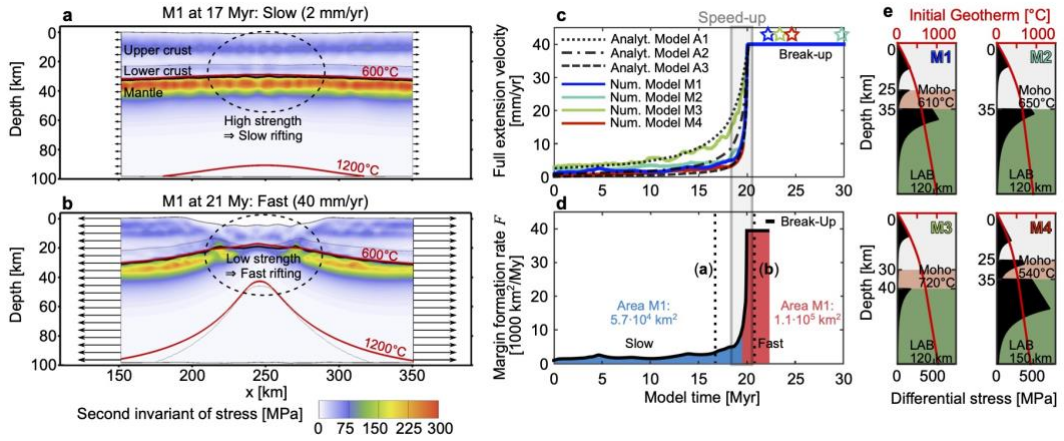

Figure 3 | Analytical and numerical model with force boundary conditions
(a,b) *Strength evolution of 2D numerical rift model. Arrows at lateral model sides indicate extension velocity.* ***(c)*** *Velocity evolution of analytical models (A1-A3) and numerical experiments (M1-M4). Analytical solution A1 employs a stress-exponent of n=3.5, assuming an entirely viscous lithosphere, while A2 and A3 also account for brittle crustal deformation by using n=10 and n=30 respectively. Numerical reference model M1 is described in the Methods and Extended Data Table 1. Other models are identical to M1, but apply a fully felsic crust (M2), a comparably thick crust (M3), or a thick lithosphere (M4), respectively. The duration of plate speed-up is a few million years for any of these configurations. The generated margin structures of M1-M4 are displayed along with 6 alternative models in Extended Data Fig. 7.* ***(d)*** *The margin area of M1 consists of two significant parts, formed during the slow and the fast phase, respectively. A constant rift length of 1000 km is assumed.* ***(e)*** *Rheological setup of models M1-M4.*

the rift becomes abandoned (Extended Data Fig. 7). We conclude that our plate kinematic and theoretical analyses independently suggest two-phase velocity behaviour as a key feature of successful rifts, which should have affected any rifted continental margin. Numerical modelling with realistic material properties as conducted here bracket the duration of rift-induced plate speed-up between 10 and 2 million years.

Our results have profound implications for the interpretation of passive margin structures. A variety of studies illustrate striking differences between proximal and distal rifted margin domains[3,10]. This dichotomy can be attributed to the suggested two-phase velocities during basin-ward localisation: the slow phase shapes the proximal margin, while the fast phase dominates the distal margin where our analysis predicts larger fault-slip rates, faster subsidence, higher heat-flow, enhanced partial melting and associated underplating or volcanism.

This study provides an alternative explanation for the often enigmatic lack of extension interpreted from the tectono-stratigraphic record along many rifted margins[17]. Both reconstructions and modelling suggest that most of the new area of crust formed during rifting is created in a comparably short period of time towards the end of the syn-rift phase, when strain is likely to have localised to the distal part of the margins. This may explain why extension estimates from syn-rift faulting, typically biased towards the proximal margin areas, and interpreted using concepts borrowed from failed rifts where the feedback process we describe never occurred, commonly underestimate the total extension indicated by whole-crustal thinning.

Our results are applicable to any rifted margin, whether volcanic or magma-poor. Yet, the evolution of specific rifts will be modulated by other factors affecting the force budget and the rift strength such as lithospheric heterogeneity, rift obliquity[13], active rifting due to asthenospheric upwelling[18], diking as well as plume arrival[19]. Plumes contribute to break-up by reducing the strength of the rift[19], however there can be a significant delay between plume arrival and abrupt plate acceleration[20]. While any combination of these processes may influence how lithospheric strength evolves within individual rift systems, all successful rifts are expected to experience the proposed strength-velocity feedback prior to breakup.

Due to the high viscosity of the lower mantle[21] only lithospheric and upper mantle processes can affect plate movements at time scales of a few million years. It has been proposed that abrupt plate accelerations can be caused by plume-lithosphere interaction[22], subduction initiation[23], and slab detachment[24] possibly induced by ridge subduction[25]. However, none of these mechanisms explains our result that plate speed-up systematically precedes continental break-up. While the present motions of Earth's plates are governed by slab pull, basal drag, and ridge push, we propose that abrupt plate acceleration during continental rifting is controlled by the rapid decrease of rift strength.

Dynamic rift weakening presents a new explanation for several previously unexplained rapid absolute plate motion changes, often appearing as cusps or kinks in apparent polar wander (APW) paths. A recent review[26] found 4 cusps in global APW paths during the last 200 million years and each of them can be associated with rift velocity speed-up during major continental rifting events: (1) 190 Myr ago - central North Atlantic opening, (2) 150 Myr ago - separation of East and West Gondwana, (3) 125 Myr ago - South Atlantic Rift and the split between India and Antarctica, (4) 50 Myr ago - North East Atlantic opening. A global-scale plate reorganisation at ~100 Myr ago[27] corresponds to an increase in rift velocity between Australia and Antarctica, and the end of a standstill in the polar wander path for South America as the final continental connection with Africa is broken[8]. We suggest that absolute plate motion changes are strongly related to continental breakup, allowing a linkage between paleomagnetic data and geological evidence in reconstructing the dynamics of previous supercontinents such as Pangea, Rodinia and Nuna.

Online Content

Methods, along with additional Extended Data display items and Supplementary Data, are available in the online version of the paper; references unique to these sections appear only in the online paper. The rift velocity database is accessible via an open-access virtual-globe web interface through https://portal.gplates.org/cesium/?view=rift_v .

References

1. Burov, E. B. in *Treatise on Geophysics Vol 6 - Crust and Lithosphere Dynamics* 99–151 (2007).
2. Whitmarsh, R. B., Manatschal, G. & Minshull, T. A. Evolution of magma-poor continental margins from rifting to seafloor spreading. *Nature* **413,** 150–154 (2001).
3. Péron-Pinvidic, G. & Manatschal, G. The final rifting evolution at deep magma-poor passive margins from Iberia-Newfoundland: a new point of view. *Int. J. Earth Sci.* **98,** 1581–1597 (2009).
4. Pérez-Gussinyé, M., Morgan, J. P., Reston, T. J. & Ranero, C. R. The rift to drift transition at non-volcanic margins: Insights from numerical modelling. *Earth Planet. Sci. Lett.* **244,** 458–473 (2006).
5. Brune, S., Heine, C., Perez-Gussinye, M. & Sobolev, S. V. Rift migration explains continental margin asymmetry and crustal hyper-extension. *Nat. Commun.* **5,** (2014).
6. Seton, M. *et al.* Global continental and ocean basin reconstructions since 200 Ma. *Earth-Sci. Rev.* **113,** 212–270 (2012).
7. Heine, C., Zoethout, J. & Müller, R. D. Kinematics of the South Atlantic rift. *Solid Earth* **4,** 215–253 (2013).
8. Granot, R. & Dyment, J. The Cretaceous opening of the South Atlantic Ocean. *Earth Planet. Sci. Lett.* **414,** 156–163 (2015).
9. Heine, C. & Brune, S. Oblique rifting of the Equatorial Atlantic: Why there is no Saharan Atlantic Ocean. *Geology* **42,** 211–214 (2014).
10. Lavier, L. L. & Manatschal, G. A mechanism to thin the continental lithosphere at magma-poor margins. *Nature* **440,** 324–328 (2006).
11. Kusznir, N. J. & Park, R. G. The extensional strength of the continental lithosphere: its dependence on geothermal gradient, and crustal composition and thickness. *Geol. Soc. Lond. Spec. Publ.* **28,** 35–52 (1987).
12. Christensen, U. R. An Eulerian technique for thermomechanical modeling of lithospheric extension. *J. Geophys. Res. Solid Earth* **97,** 2015–2036 (1992).
13. Brune, S., Popov, A. A. & Sobolev, S. V. Modeling suggests that oblique extension facilitates rifting and continental break-up. *J. Geophys. Res.* **117,** B08402 (2012).
14. Bürgmann, R. & Dresen, G. Rheology of the Lower Crust and Upper Mantle: Evidence from Rock Mechanics, Geodesy, and Field Observations. *Annu. Rev. Earth Planet. Sci.* **36,** 531–567 (2008).
15. Takeshita, T. & Yamaji, A. Acceleration of continental rifting due to a thermomechanical instability. *Tectonophysics* **181,** 307–320 (1990).
16. Hopper, J. R. & Buck, W. R. The initiation of rifting at constant tectonic force: Role of diffusion creep. *J. Geophys. Res. Solid Earth* **98,** 16213–16221 (1993).
17. Reston, T. J. The structure, evolution and symmetry of the magma-poor rifted margins of the North and Central Atlantic: A synthesis. *Tectonophysics* **468,** 6–27 (2009).
18. Huismans, R. S., Podladchikov, Y. Y. & Cloetingh, S. Transition from passive to active rifting: Relative importance of asthenospheric doming and passive extension of the lithosphere. *J. Geophys. Res. Solid Earth* **106,** 11271–11291 (2001).

19. Buiter, S. J. H. & Torsvik, T. H. A review of Wilson Cycle plate margins: A role for mantle plumes in continental break-up along sutures? *Gondwana Res.* **26,** 627–653 (2014).
20. Brune, S., Popov, A. A. & Sobolev, S. V. Quantifying the thermo-mechanical impact of plume arrival on continental break-up. *Tectonophysics* **604,** 51–59 (2013).
21. Hager, B. H. & Richards, M. A. Long-Wavelength Variations in Earth's Geoid: Physical Models and Dynamical Implications. *Philos. Trans. R. Soc. Lond. Math. Phys. Eng. Sci.* **328,** 309–327 (1989).
22. Cande, S. C. & Stegman, D. R. Indian and African plate motions driven by the push force of the Reunion plume head. *Nature* **475,** 47–52 (2011).
23. Gurnis, M., Hall, C. & Lavier, L. Evolving force balance during incipient subduction. *Geochem. Geophys. Geosystems* **5,** 33 PP. (2004).
24. Bercovici, D., Schubert, G. & Ricard, Y. Abrupt tectonics and rapid slab detachment with grain damage. *Proc. Natl. Acad. Sci.* **112,** 1287–1291 (2015).
25. Seton, M. *et al.* Ridge subduction sparked reorganization of the Pacific plate-mantle system 60-50 million years ago. *Geophys. Res. Lett.* 2015GL063057 (2015). doi:10.1002/2015GL063057
26. Torsvik, T. H., Muller, R. D., Van der Voo, R., Steinberger, B. & Gaina, C. Global plate motion frames: Toward a unified model. *Rev. Geophys.* **46,** (2008).
27. Matthews, K. J., Seton, M. & Müller, R. D. A global-scale plate reorganization event at 105−100 Ma. *Earth Planet. Sci. Lett.* **355–356,** 283–298 (2012).

Acknowledgements

S.B. was funded by the Marie Curie International Outgoing Fellowship 326115, the German Research Foundation Priority Program 1375 SAMPLE, and the Helmholtz Young Investigators Group CRYSTALS. S.E.W., N.P.B. and R.D.M. were supported by SIEF project RP 04-174 and ARC grant IH130200012. Simulations were performed on the GFZ Potsdam cluster. Figures were created using matplotlib, Tecplot, and Matlab. We thank Xiaodong Qin and John Cannon for their efforts developing the GPlates portal and pyGPlates infrastructure.

Author Contributions

S.B. and S.E.W. conceived the plate tectonic analysis. S.B. designed and conducted the thermo-mechanical modeling. S.B., S.E.W., and N.P.B. developed the pyGPlates workflow. S.B., S.E.W., and R.D.M. discussed and integrated the results. The paper was written by S.B., with contributions from all authors.

Additional Information

Reprints and permissions information is available at www.nature.com/reprints. The authors declare no competing financial interests. Readers are welcome to comment on the online version of the paper. Correspondence and requests for materials should be addressed to S.B. (sascha.brune@gfz-potsdam.de).

Methods

The methods section summarizes the rationale behind the chosen regional kinematic models, and how we derive the set of continent-ocean boundaries. We refer to observational evidence of the onset of rifting for each of the eight studied rift zones and compare alternative South Atlantic plate models. Finally, we describe the applied methods for numerical and analytical solutions for constant-force extension of a power-law lithosphere.

Rift Kinematics

Quantitative restoration of continents to their pre-rift configuration during Pangea breakup involves estimating the amount of syn-rift extension from present-day crustal thickness, and accounting for uncertainties in these estimates[28,29]. The time of onset of rifting between two plates is constrained by geological evidence such as the ages of oldest syn-rift sediments and rift-associated volcanism. The direction and rate of divergence during rifting can be reconstructed by careful consideration of a diverse range of geological indicators such as seismic tectono-stratigraphy, dating of exhumed and volcanic rocks dredged/drilled within continent-ocean transitions, and fitting constraints from sections of the plate boundaries beyond the rift zone[7,30,31]. Note that in Mesozoic/Cenozoic tectonic reconstructions, plate rotations have to be discretized, whereas typical stage lengths are 5 to 10 million years or even longer as observations usually don't permit building plate kinematic models with smaller stages. Our analysis combines independently conducted reconstructions (Supplementary Table 1) that account for recent geological and geophysical data sets.

Continent-Ocean Boundaries (COBs)

The definition of COBs contains significant uncertainties for many margins - indeed, the definition of a COB as a sharp boundary is conceptually problematic, with interpretations of geophysical data highlighting the complex crustal architecture within the transition from continental to oceanic domains[2,32]. Regions of transition can be several tens of km wide, with complexities that vary between margins closer to volcanic or non-volcanic end-member scenarios. As with the plate kinematic model, our starting point for defining COBs were the geometries defined by Seton et al. (2012)[6]. We modified these using a synthesis of COB interpretations compiled from published crustal-scale geophysical data sets (see Supplementary Table 2). These data are primarily derived from seismic refraction experiments, but interpretations of crustal structure based on seismic reflection and gravity modelling are also included for regions where refraction data are sparse. Additional seismic constraints come from the data set of Winterbourne et al. (2009)[33], who identified unequivocal oceanic crust adjacent to continental margins along seismic profiles including some industry data, which are otherwise unavailable. The synthesis of margin-perpendicular profiles gives us a series of tie points along each margin, with which our COBs must be broadly consistent. To define COB polylines, we must interpolate between these tie points, which we did guided by first order trends in maps of gravity derivatives and magnetic anomalies[29].

However, for the specific purposes of this study, an important consideration is that we use the COBs to define the orientation of the rift. For this reason, we have used deliberately simplified COB geometries with orientations that represent the first order trend of each rifted margin. Using these constraints, we generated alternative COB geometries to define a range of possible COB locations. Our preferred COB set lies relatively ocean-ward, so that it includes areas where the basement is interpreted to comprise exhumed mantle or seaward dipping reflectors, but not basement formed by seafloor spreading processes. To test how sensitive our results are to our COB interpretation, we generated a second set of COB geometries, defining the extreme landward limit of basement that is not clearly continental crust (see Extended Data Fig. 1 and 3).

Observational evidence for timing of rift initiation

Our results, and particularly the occurrence of a two-phase, 'slow-fast' pattern in reconstructions of continental rifting, is sensitive to the age assigned to the onset of rifting. The condition for the slow-fast trend to disappear would be if the rift onset ages in our reconstruction model are erroneously old, such that rifting began later and proceeded (from the same full-fit configuration) at a faster rate. Hence, to establish the robustness of the slow-fast trend, we summarize geological evidence for the minimum age at which rifting began in each of the rift systems illustrated in our study, as well as observational evidence for accelerations in rift velocity that lend weight to our kinematic reconstructions.

South Atlantic Rift

We model South Atlantic rifting using the reconstruction of Heine et al (2013)[7], with onset of slow rifting at ~150 Myr ago followed by acceleration at ~125 Myr ago. An extensive study linking biostratigraphy, lithostratigraphy and timing of deformation within basins along both African and South Atlantic conjugate margins north of the Walvis Fracture Zone[34] indicates that rifting was established by Berriasian times (>140 Myr ago). South of the Walvis Fracture Zone, the main phase of rifting between South America and southern Africa likely began earlier, in the Late Jurassic, following widespread, isolated Triassic-Jurassic rift basin development within southern South America[35]. The timing of slow rift onset and subsequent acceleration are consistent with earlier reconstructions[36]. A reconstruction invoking later, post-Aptian age of breakup between salt basins on the Brazilian and Angolan conjugate margins[37] has been proposed, but detailed seismic imaging and drilling of syn-rift sediments within the rifted margins, combined with basin subsidence histories[38] argue against this later breakup scenario. Further supporting our model, recent interpretation of magnetic anomalies in the southern South Atlantic within crust formed during the Cretaceous Normal Superchron constrains changes in the rate and direction of plate motions during breakup[8], showing rapid acceleration of plate divergence during initial breakup in the southernmost South Atlantic, contemporaneous with the final stages of rifting further north.

Central North Atlantic Rift

Our base reconstruction follows the work of Kneller et al (2012)[28], who assigned a rifting onset age of 240 Myr ago, and predicts a speed-up at ~200 Myr ago. The speed-up occurs around the time of Central Atlantic Magmatic Province (CAMP) volcanism, which represents an important time marker within the rift evolution. Stratigraphic evidence from syn-rift sediments within basins along the eastern margins of North America[39,40] and the conjugate Northwest African margins[41] shows that continental rifting was active for at least 25 Myr prior to CAMP magmatism. Rapid speed-up of rifting is evidenced by a rate of sediment accumulation within these basins that increases significantly within 1 to 5 million years shortly before 200 Myr ago[39].

North America - Iberia

Our reconstruction proceeds from onset of rifting at 200 Myr ago with a speed-up at ~145 Myr ago. Recent, alternative reconstructions[42] show a similar increase in extension velocities at the end of the Jurassic, but with a slightly earlier initiation of rifting (~203 Myr ago). Evidence for widespread rifting is recorded in basins along the Newfoundland and Iberian margins beginning in the late Triassic, but resulting in little crustal thinning; a second phase beginning in the late Jurassic lead to significant thinning and breakup in the Early Cretaceous[43,44]. Sequential restoration[45] yields post-145 Myr ago extension velocities of 1-2 mm/yr, consistent with our reconstructions. The rift velocity prior to ~145 Myr ago depends on the assumed age of rift onset. Taking the latest possible onset of rifting, Oxfordian (~161 Myr ago), modelled extension rates remain fairly constant throughout rifting. However, any earlier onset of rifting (e.g. Triassic-Early Jurassic) as indicated by evidence listed above, would result in slower initial rifting followed by a Late Jurassic acceleration, consistent with our reconstruction model. The slow-fast velocity evolution is further supported by a study[46] that uses previously unpublished seismic and borehole data to show continuous rifting in the basins along western Iberia beginning in the Triassic (>210 Myr ago), with three rift cycles, ending at 144 Myr ago. These authors find that the subsidence is relatively slow in the first two rift phases, then increases rapidly in rate during a rift climax in Late Oxfordian-Kimmeridgian times (~160-152 Myr ago) coinciding with the timing of our speed-up.

Australia - Antarctica

Our reconstruction places the onset of rifting between Australia and Antarctica in the late Jurassic (~165-155 Myr ago), with an increase in rift velocity around 100 Myr ago. The earliest rift-fill comprises Callovian - Early Berriasian sediments (>160 to ~140 Myr ago), constrained by palynological dating of samples from the Polda, Bremer, and Eyre basin[47]. Detailed tectono-stratigraphic analysis[47] and sequential structural restoration of interpreted seismic sections[48] point towards slow rifting during the Jurassic-Early Cretaceous, followed by a rapid acceleration in crustal thinning and subsidence at the beginning of the Late Cretaceous (beginning around 102 or 93.5 Myr ago)[48,49]. Shortly thereafter, breakup begins in the westernmost part of the rift system (dated by exhumation fabrics and volcanics), propagating eastwards over 10s of millions of years[50].

South China Sea

Reconstructions of the South China margins indicate rapid extension and breakup beginning in the late Eocene[51]. Earlier extension developed from ~60 Myr ago within a former Andean-style margin, while onset of slow extension prior to the late Eocene speed-up is recorded by minor volcanism in rift-related basins[52]. This is further supported by subsidence and strain-rate analyses of wells and stratigraphic sections for basins within the northern margin of the South China Sea[53].

Gulf of California

The speed-up in our reconstruction occurs around 12 Myr ago, corresponding to a phase of abruptly increased rift velocity and obliquity inferred from widespread structural markers[54]. Phases of continental extension before the mid-Miocene are recorded by tectono-stratigraphic relationships and dating of rift-related volcanics and plutons[55,56]. These data indicate more diffuse extension at significantly lower rates: Ferrari et al (2013)[55] estimate that the relative motion between the conjugate margins of the Gulf of California proceeded at an average of 7.7 mm/yr from ~30-18 Myr ago, and 8.3 mm/yr from ~18-12 Myr ago, consistent with our computed values.

North America - Greenland

Initiation of rifting by ~140 Myr ago is substantiated by dating of rift-related volcanics and biostratigraphy[57]. Starting from ~120 Myr ago, rift basin sedimentation is evident throughout the Cretaceous[58]. Rifting and subsidence rates were slow until a rapid increase around 70-80 Myr ago[57,59], around the time of an increase in rift velocity and subsequent initiation of seafloor spreading.

North East Atlantic

Our reconstruction of relative motion between Greenland and Eurasia prior to the oldest seafloor spreading magnetic anomalies in the NE Atlantic (C24, ~53 Myr ago[60]) incorporates plate circuit computations using constraints from the rift systems between Greenland, North America and Eurasia. The reconstruction shows slow extension in the Jurassic to Early Cretaceous followed by tectonic quiescence or modest mid-Cretaceous extension[61,62], and a significant speed-up in the Late Cretaceous. The acceleration in Late Cretaceous rifting indicated by the reconstructions is more tightly constrained from spreading histories in the adjacent basins. The most significant phase of rifting that ultimately lead to breakup is constrained to the Latest Cretaceous-Early Paleocene. Skogseid (1994)[63] proposed that enhanced syn-rift deposition took place between 75 and 62 Myr ago based on tectono-stratigraphy and subsidence analysis from seismic and well data from the Vøring margin.

End-member models of the South Atlantic Rift

We performed our analysis on several end-member models for the South Atlantic Rift (Extended Data Fig. 8). These models differ in terms of the timing of final South Atlantic break-up, which is difficult to constrain due to the Cretaceous superchron. However, models that feature a late break-up[8,37,64]

also show a late speed-up at 110 Myr ago. Models with an earlier break-up, however[7,36] depict an earlier speed-up at 120 Myr ago. In all cases, initially slow rift velocities are followed by large plate accelerations that precede the final break-up by 10-15 million years.

Another major difference between these models is the plate-internal deformation within South America: the Heine et al. (2013) model[7] uses a largely intact South American plate where deformation occurs only along the border to Patagonia, while Moulin et al. (2010)[64] separate South America in 8 individual plates. We apply our analysis under two premises: (1) assuming a three-plate scenario (West Africa, South Africa, South America) shown in the upper panel of rift velocity diagrams (Extended Data Fig. 8b), (2) we account for South America-internal deformation in a four-plate analysis where the northern and the southern part of South America are evaluated independently within the two lowermost panels in Extended Data Fig. 8b.

We find that plate models, which feature large intra-plate deformation[36,37,64] display two significant speed-up events: first the Southern plates accelerate several million years prior to break-up in the Southern South Atlantic and secondly the Northern plates accelerate prior to break-up in the equatorial Atlantic. Plate models with less internal deformation such as the Heine et al. (2013) model displays only a minor acceleration prior to Southern South Atlantic opening whereas the largest speed-up occurs at 120 Myr ago prior to equatorial Atlantic break-up. While the relative importance of each speed-up depends on the amount of South America-internal deformation, all models illustrate plate acceleration prior to break-up of the controlling rift segment.

Database

The entire rift velocity database is accessible via an open-access virtual-globe web interface through https://portal.gplates.org/cesium/?view=rift_v. This database contains the rift velocity history of any point at a major post-Pangea rifted margin. The velocity history can be visualized online and downloaded, lending itself as a source of tectonic boundary conditions for basin analysis software and geodynamic forward models.

Numerical Model Setup

We apply the finite element code SLIM3D[65] to solve the coupled system of conservation equations for momentum, thermal energy and constitutive equations. The reference model M1 consists of four distinct petrological layers: 25 km of felsic upper crust[66], 10 km of mafic lower crust[67], and a lithospheric mantle dominated by dry olivine rheology[68] that extends to a depth of 120 km. The weak asthenospheric material below 120 km depth is represented through wet (i.e., 1000 ppm H/Si) olivine rheology[68]. The entire model comprises a rectangular domain of 150 km depth and 500 km width, with 2 km resolution.

We apply dynamic boundary conditions at the lateral model sides, such that during rifting, the boundary force is kept constant allowing for self-consistent evolution of extensional velocities. This approach is feasible if the model domain represents a large region whose strength is a major component in the overall force balance of the involved plates. The constant boundary force is

maintained in our model until extensional velocities reach typical sea-floor spreading rates. Hereafter, the low rift strength becomes neglectable in the force balance, and we use velocity boundary conditions with a rate of 40 mm/yr. At the top boundary we use a free surface while at the bottom side isostatic equilibrium is realized by means of the Winkler foundation, where in- and outflow of material is accounted for during re-meshing. Deformation is accommodated by elasto-visco-plastic rheology so that the model self-consistently reproduces diverse lithospheric-scale deformation processes like faulting, flexure and lower crustal flow. Viscous flow occurs via two creep mechanisms: diffusion and dislocation creep. The Mohr-Coulomb failure model is implemented for brittle deformation.

The thermal state at the model start is a steady-state temperature distribution resulting from each layer's heat conductivity, radiogenic heat production and the following boundary conditions: (1) lateral boundaries are thermally isolated, (2) the temperature at the surface is 0 °C, (3) below the lithosphere asthenosphere boundary the temperature is set to 1,350 °C. In order to avoid rift localization at the model boundaries, a small thermal heterogeneity is introduced in the model centre. We introduce this heterogeneity of triangular shape and 20 km width by elevating the initial 1,350 °C isotherm up to 10 km prior to thermal equilibration[5]. All rheological and thermal parameters are given in Extended Data Tab. 1.

Analytical solution

Here we derive a transparent analytical solution for finite amplitude necking of a homogeneous viscous layer consisting of a power-law material. A horizontal layer of initial thickness D is extended by a constant line force F that is applied parallel to the layer. In an incompressible, free layer the mean layer-parallel deviatoric stress τ is half of the total stress, F/D_0 (Ref. 69), i.e. $\tau=1/2\ F/D_0$. The deviatoric stress further relates to the strain rate through the power law $\dot{e} = B\ \tau^n$ where the pre-exponential factor B and the stress exponent n are material parameters. Note that B is often considered to be temperature-dependent with $B=A\ \cdot exp(-E/(RT))$. Based on these relations a characteristic viscosity $\eta_c = \tau/\dot{e} = \tau^{(1-n)}/B$ and a characteristic time $t_c = \eta_c / \tau = 1/B\ \cdot (1/2\ F/D_0)^{-n}$ can be defined[70].

Due to mass conservation in incompressible flow, the horizontal stretching of the layer has to be balanced by vertical thinning: $1/L\ dL/dt = -1/D\ dD/dt$, where L is the length of the layer. The resulting extensional velocity $v = dL/dt$ can thus be written as

$$v = -L/D\ dD/dt \qquad \text{Eq. 1}$$

We assume that the upper and lower boundaries are traction-free and that no depth-dependent thinning occurs. These assumptions allowed derivation of closed analytical solutions for necking instabilities in boudinage mechanics and slab-detachment[70] involving the time-dependent layer thickness D that can be expressed as:

$$D = D_0\ (1-t/t_r)^{(1/n)} \qquad \text{Eq. 2}$$

where the time until rupture t_r relates to the aforementioned characteristic time[70] t_c such that $t_r = t_c/n$.

Combining Eq. 1 and Eq. 2 yields the formula for the time-dependent extension velocity:

$$v = L/(n\, t_r) \cdot (1-t/t_r)^{-1} \qquad \text{Eq. 3}$$

In order to apply the analytical results to continental rifting, we use parameters that describe a typical rift configuration (lithospheric thickness: 100 km, mean lithospheric temperature T=600 °C, applied tectonic force: 8 TN/m, width of the necking zone L=100 km, duration of rifting t_r=20 Myr). The stress exponents of lithospheric materials range between 3 and 4, hence a purely viscous lithosphere can be approximated by n=3.5. However, this approach neglects the existence of brittle deformation that is evidenced at real plate boundaries by ubiquitous faulting. Brittle failure can be represented as an end-member of power law creep, if stress exponents up to 30 are used[12]. The analytical solution is plotted in Fig. 3 for three cases: n=3.5 (A1), n=10 (A2), n=30 (A3). Despite the simplicity of the analytical model, the numerical solutions of lithospheric necking are very similar to analytical solutions (Fig. 3). Hence, the analytical calculation corroborates our conclusion that it is the rapid loss of lithospheric strength during continental rifting, which is responsible for the abrupt increase of extension velocity.

Methods References

28. Kneller, E. A., Johnson, C. A., Karner, G. D., Einhorn, J. & Queffelec, T. A. Inverse methods for modeling non-rigid plate kinematics: Application to mesozoic plate reconstructions of the Central Atlantic. *Comput. Geosci.* **49,** 217–230 (2012).
29. Williams, S. E., Whittaker, J. M. & Müller, R. D. Full-fit, palinspastic reconstruction of the conjugate Australian-Antarctic margins. *Tectonics* **30,** 21 PP. (2011).
30. Sutra, E., Manatschal, G., Mohn, G. & Unternehr, P. Quantification and restoration of extensional deformation along the Western Iberia and Newfoundland rifted margins. *Geochem. Geophys. Geosystems* n/a–n/a (2013). doi:10.1002/ggge.20135
31. Whittaker, J. M., Williams, S. E. & Müller, R. D. Revised tectonic evolution of the Eastern Indian Ocean. *Geochem. Geophys. Geosystems* **14,** 1891–1909 (2013).
32. Dean, S. L., Sawyer, D. S. & Morgan, J. K. Galicia Bank ocean–continent transition zone: New seismic reflection constraints. *Earth Planet. Sci. Lett.* **413,** 197–207 (2015).
33. Winterbourne, J., Crosby, A. & White, N. Depth, age and dynamic topography of oceanic lithosphere beneath heavily sedimented Atlantic margins. *Earth Planet. Sci. Lett.* **287,** 137–151 (2009).
34. Chaboureau, A.-C. *et al.* Paleogeographic evolution of the central segment of the South Atlantic during Early Cretaceous times: Paleotopographic and geodynamic implications. *Tectonophysics* **604,** 191–223 (2013).

35. Loegering, M. J. *et al.* Tectonic evolution of the Colorado Basin, offshore Argentina, inferred from seismo-stratigraphy and depositional rates analysis. *Tectonophysics* **604,** 245–263 (2013).
36. Nürnberg, D. & Müller, R. D. The Tectonic Evolution of the South-Atlantic from Late Jurassic to Present. *Tectonophysics* **191,** 27–53 (1991).
37. Torsvik, T. H., Rousse, S., Labails, C. & Smethurst, M. A. A new scheme for the opening of the South Atlantic Ocean and the dissection of an Aptian salt basin. *Geophys. J. Int.* **177,** 1315–1333 (2009).
38. Quirk, D. G. *et al.* Rifting, subsidence and continental break-up above a mantle plume in the central South Atlantic. *Geol. Soc. Lond. Spec. Publ.* **369,** 185–214 (2013).
39. Schlische, R. W., Withjack, M. O. & Olsen, P. E. Relative timing of CAMP, rifting, continental breakup, and basin inversion: Tectonic significance. *Geophys. Monogr.* **136,** 33–59 (2003).
40. Withjack, M. O., Schlische, R. W., Malinconico, M. L. & Olsen, P. E. Rift-basin development: lessons from the Triassic–Jurassic Newark Basin of eastern North America. *Geol. Soc. Lond. Spec. Publ.* **369,** 301–321 (2013).
41. Davison, I. Central Atlantic margin basins of North West Africa: Geology and hydrocarbon potential (Morocco to Guinea). *J. Afr. Earth Sci.* **43,** 254–274 (2005).
42. Vissers, R. L. M., van Hinsbergen, D. J. J., Meijer, P. T. & Piccardo, G. B. Kinematics of Jurassic ultra-slow spreading in the Piemonte Ligurian ocean. *Earth Planet. Sci. Lett.* **380,** 138–150 (2013).
43. Péron-Pinvidic, G. & Manatschal, G. The final rifting evolution at deep magma-poor passive margins from Iberia-Newfoundland: a new point of view. *Int. J. Earth Sci.* **98,** 1581–1597 (2009).
44. Alves, T. M. *et al.* Diachronous evolution of Late Jurassic–Cretaceous continental rifting in the northeast Atlantic (west Iberian margin). *Tectonics* **28,** TC4003 (2009).
45. Sutra, E., Manatschal, G., Mohn, G. & Unternehr, P. Quantification and restoration of extensional deformation along the Western Iberia and Newfoundland rifted margins. *Geochem. Geophys. Geosystems* 14 (2013). doi:10.1002/ggge.20135
46. Pereira, R. & Alves, T. M. Tectono-stratigraphic signature of multiphased rifting on divergent margins (deep-offshore southwest Iberia, North Atlantic). *Tectonics* **31,** TC4001 (2012).
47. Ball, P., Eagles, G., Ebinger, C., McClay, K. & Totterdell, J. The spatial and temporal evolution of strain during the separation of Australia and Antarctica. *Geochem. Geophys. Geosystems* **14,** 2771–2799 (2013).
48. Espurt, N. *et al.* Transition from symmetry to asymmetry during continental rifting: an example from the Bight Basin–Terre Adélie (Australian and Antarctic conjugate margins). *Terra Nova* **24,** 167–180 (2012).
49. Veevers, J. J. Change of tectono-stratigraphic regime in the Australian plate during the 99 Ma (mid-Cretaceous) and 43 Ma (mid-Eocene) swerves of the Pacific. *Geology* **28,** 47–50 (2000).
50. Direen, N. G., Stagg, H. M. J., Symonds, P. A. & Norton, I. O. Variations in rift symmetry: cautionary examples from the Southern Rift System

(Australia–Antarctica). *Geol. Soc. Lond. Spec. Publ.* **369,** 453–475 (2013).
51. Lee, T.-Y. & Lawver, L. A. Cenozoic plate reconstruction of the South China Sea region. *Tectonophysics* **235,** 149–180 (1994).
52. Yan, Q., Shi, X. & Castillo, P. R. The late Mesozoic–Cenozoic tectonic evolution of the South China Sea: A petrologic perspective. *J. Asian Earth Sci.* **85,** 178–201 (2014).
53. Xie, H. *et al.* Cenozoic Tectonic Subsidence in Deepwater Sags in the Pearl River Mouth Basin, Northern South China Sea. *Tectonophysics* (2014). doi:10.1016/j.tecto.2014.01.010
54. Bennett, S. E. K. & Oskin, M. E. Oblique rifting ruptures continents: Example from the Gulf of California shear zone. *Geology* **42,** 215–218 (2014).
55. Ferrari, L. *et al.* Late Oligocene to Middle Miocene rifting and synextensional magmatism in the southwestern Sierra Madre Occidental, Mexico: The beginning of the Gulf of California rift. *Geosphere* GES00925.1 (2013). doi:10.1130/GES00925.1
56. Duque-Trujillo, J. *et al.* Timing of rifting in the southern Gulf of California and its conjugate margins: Insights from the plutonic record. *Geol. Soc. Am. Bull.* **127,** 702–736 (2015).
57. Dickie, K., Keen, C. E., Williams, G. L. & Dehler, S. A. Tectonostratigraphic evolution of the Labrador margin, Atlantic Canada. *Mar. Pet. Geol.* **28,** 1663–1675 (2011).
58. Chalmers, J. A. & Pulvertaft, T. C. R. Development of the continental margins of the Labrador Sea: a review. *Geol. Soc. Lond. Spec. Publ.* **187,** 77–105 (2001).
59. McGregor, E. D., Nielsen, S. B., Stephenson, R. A. & Haggart, J. W. Basin evolution in the Davis Strait area (West Greenland and conjugate East Baffin/Labrador passive margins) from thermostratigraphic and subsidence modelling of well data: Implications for tectonic evolution and petroleum systems. *Bull. Can. Pet. Geol.* **62,** 311–329 (2014).
60. Gaina, C., Gernigon, L. & Ball, P. Palaeocene–Recent plate boundaries in the NE Atlantic and the formation of the Jan Mayen microcontinent. *J. Geol. Soc.* **166,** 601–616 (2009).
61. Tsikalas, F., Faleide, J. I., Eldholm, O. & Wilson, J. Late Mesozoic–Cenozoic structural and stratigraphic correlations between the conjugate mid-Norway and NE Greenland continental margins. *Geol. Soc. Lond. Pet. Geol. Conf. Ser.* **6,** 785–801 (2005).
62. Færseth, R. B. & Lien, T. Cretaceous evolution in the Norwegian Sea—a period characterized by tectonic quiescence. *Mar. Pet. Geol.* **19,** 1005–1027 (2002).
63. Skogseid, J. Dimensions of the Late Cretaceous-Paleocene Northeast Atlantic rift derived from Cenozoic subsidence. *Tectonophysics* **240,** 225–247 (1994).
64. Moulin, M., Aslanian, D. & Unternehr, P. A new starting point for the South and Equatorial Atlantic Ocean. *Earth-Sci. Rev.* **98,** 1–37 (2010).
65. Popov, A. A. & Sobolev, S. V. SLIM3D: A tool for three-dimensional thermo mechanical modeling of lithospheric deformation with elasto-visco-plastic rheology. *Phys. Earth Planet. Inter.* **171,** 55–75 (2008).

66. Gleason, G. C. & Tullis, J. A Flow Law for Dislocation Creep of Quartz Aggregates Determined with the Molten-Salt Cell. *Tectonophysics* **247,** 1–23 (1995).
67. Rybacki, E. & Dresen, G. Dislocation and diffusion creep of synthetic anorthite aggregates. *J. Geophys. Res.* **105,** 26,017–26,036 (2000).
68. Hirth, G. & Kohlstedt, D. L. Rheology of the upper mantle and the mantle wedge: A view from the experimentalists. *Geophys. Monogr.* **138,** 83–105 (2003).
69. Turcotte, D. L. & Schubert, G. *Geodynamics*. (Cambridge University Press, 2002).
70. Schmalholz, S. M. A simple analytical solution for slab detachment. *Earth Planet. Sci. Lett.* **304,** 45–54 (2011).
71. Ranalli, G. & Murphy, D. C. Rheological stratification of the lithosphere. *Tectonophysics* **132,** 281–295 (1987).

Extended Data Items

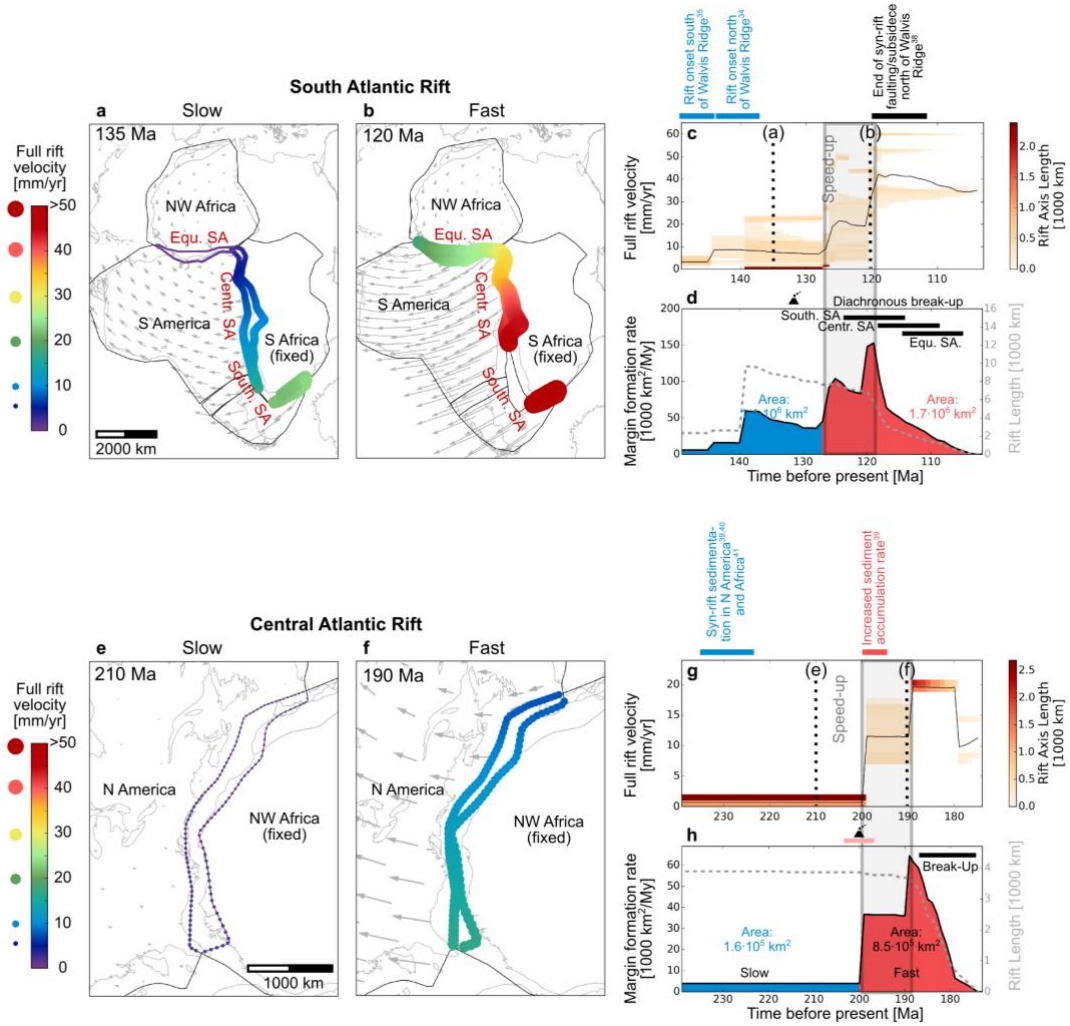

Extended Data Figure 1 | South Atlantic Rift (a-d) and the central North Atlantic Rift (e-h). *The maps depict snapshots of the slow and fast rift phase. We corroborate the inferred velocity history with key temporal constraints from geological and geophysical observations.*

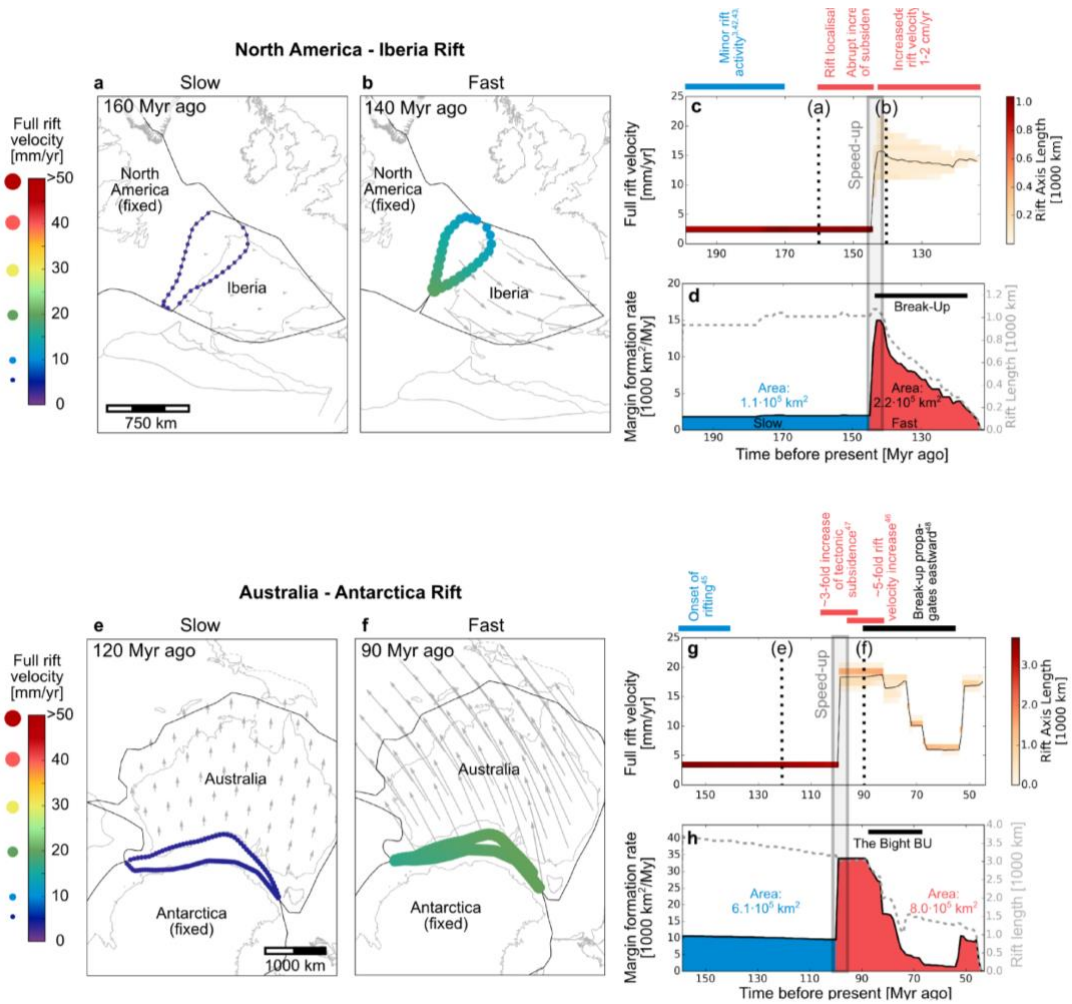

Extended Data Figure 2 | North America – Iberia Rift (a-d) and the Australia – Antarctica Rift (e-h). *The maps depict snapshots of the slow and fast rift phase. We corroborate the inferred velocity history with key temporal constraints from geological and geophysical observations.*

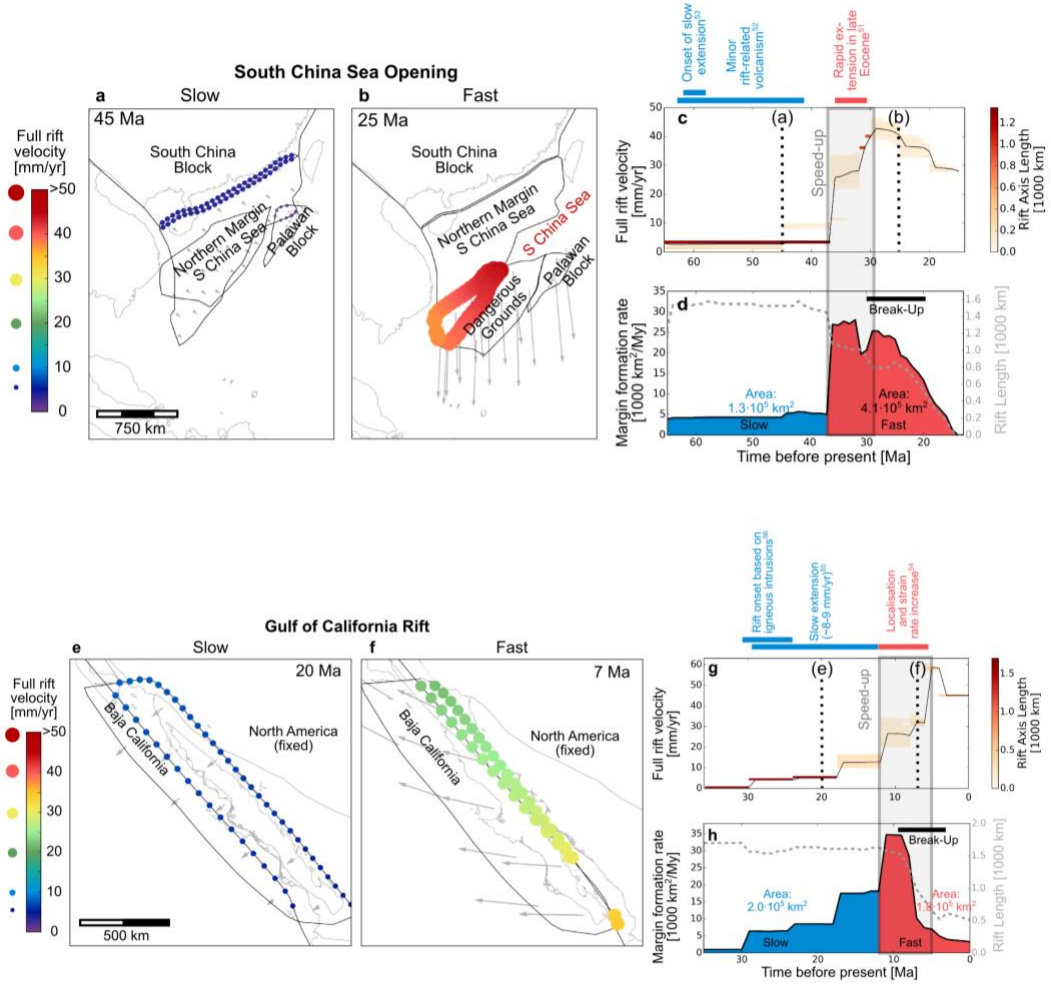

Extended Data Figure 3 | South China Sea opening (a-d) and the Gulf of California Rift (e-h). *The maps depict snapshots of the slow and fast rift phase. We corroborate the inferred velocity history with key temporal constraints from geological and geophysical observations.*

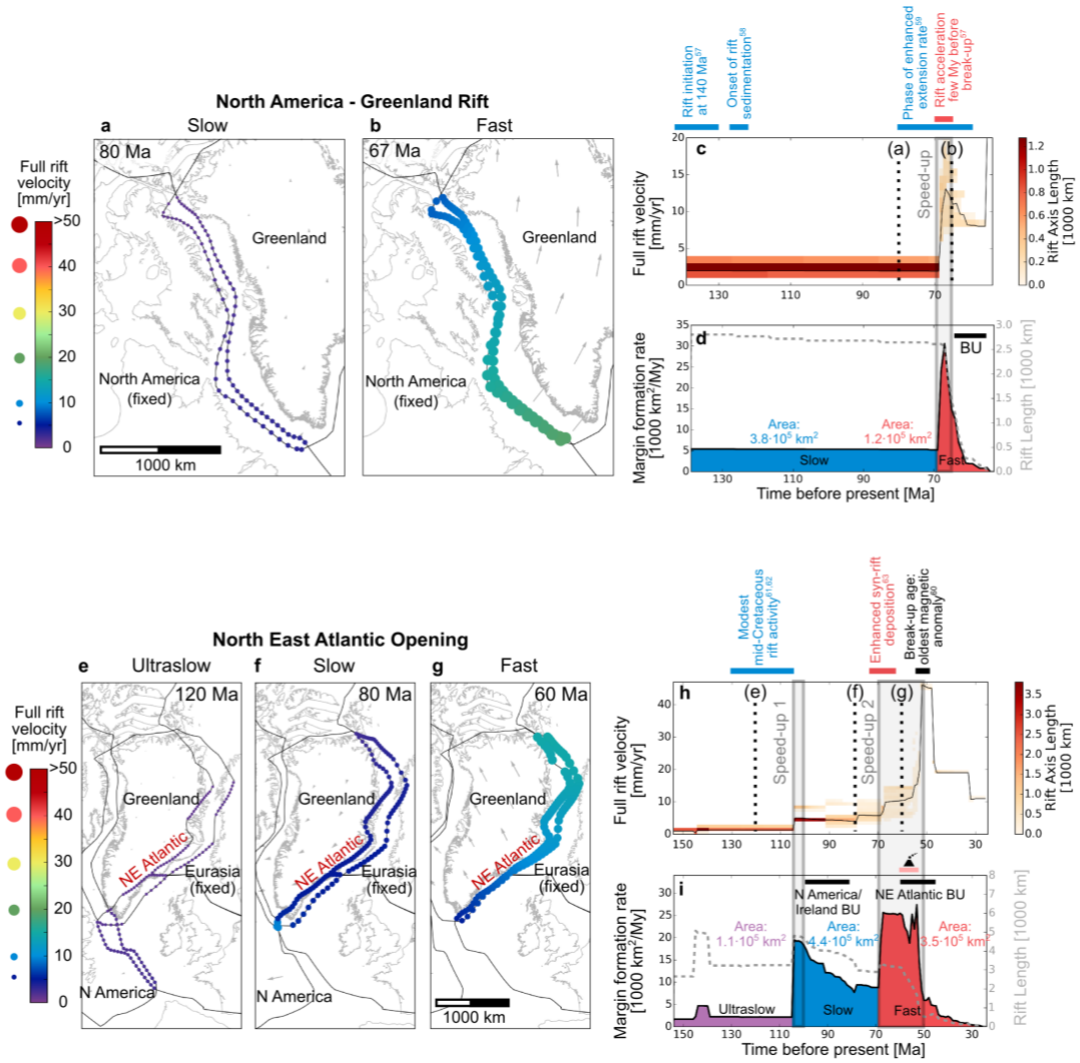

Extended Data Figure 4 | North America – Greenland Rift (a-d) and the North East Atlantic opening (e-i). *The maps depict snapshots of the slow and fast rift phase. We corroborate the inferred velocity history with key temporal constraints from geological and geophysical observations.*

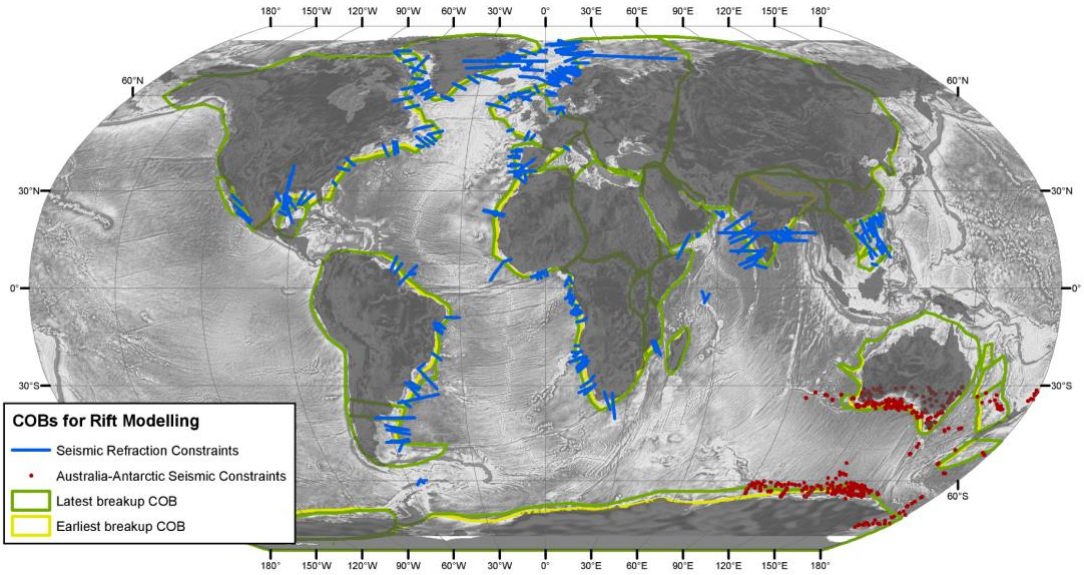

Extended Data Figure 5 | Data coverage for construction of COBs. *We restrict our analysis to regions where seismic refraction data for both conjugate margins is available. Seismic refraction profiles are shown in blue, together with 'point' deep crustal seismic soundings linked together by gravity modelling. Red points represent a mixture of sonobuoys and deep reflection profiles. All references for displayed data are listed in Supplementary Table 2. Our preferred set of COBs (green) includes some areas where the basement is interpreted to comprise exhumed mantle or seaward dipping reflectors, but not basement formed by seafloor spreading processes. The alternative set of COB geometries, defining the extreme landward limit of what basement that is not clearly continental crust, is shown in yellow*

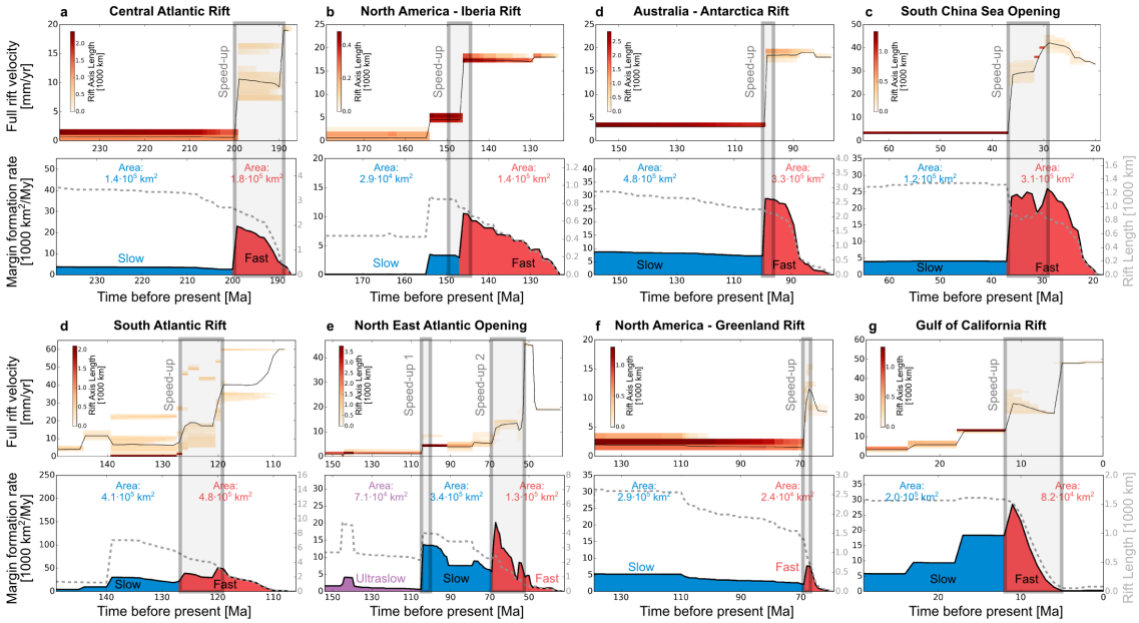

Extended Data Figure 6 | Results using alternative, continent-ward set of COBs. *The COB set is shown in Extended Data Fig. 5 as yellow polygons. Break-up takes place earlier, yet the two-phase evolution is robustly represented in this end-member scenario.*

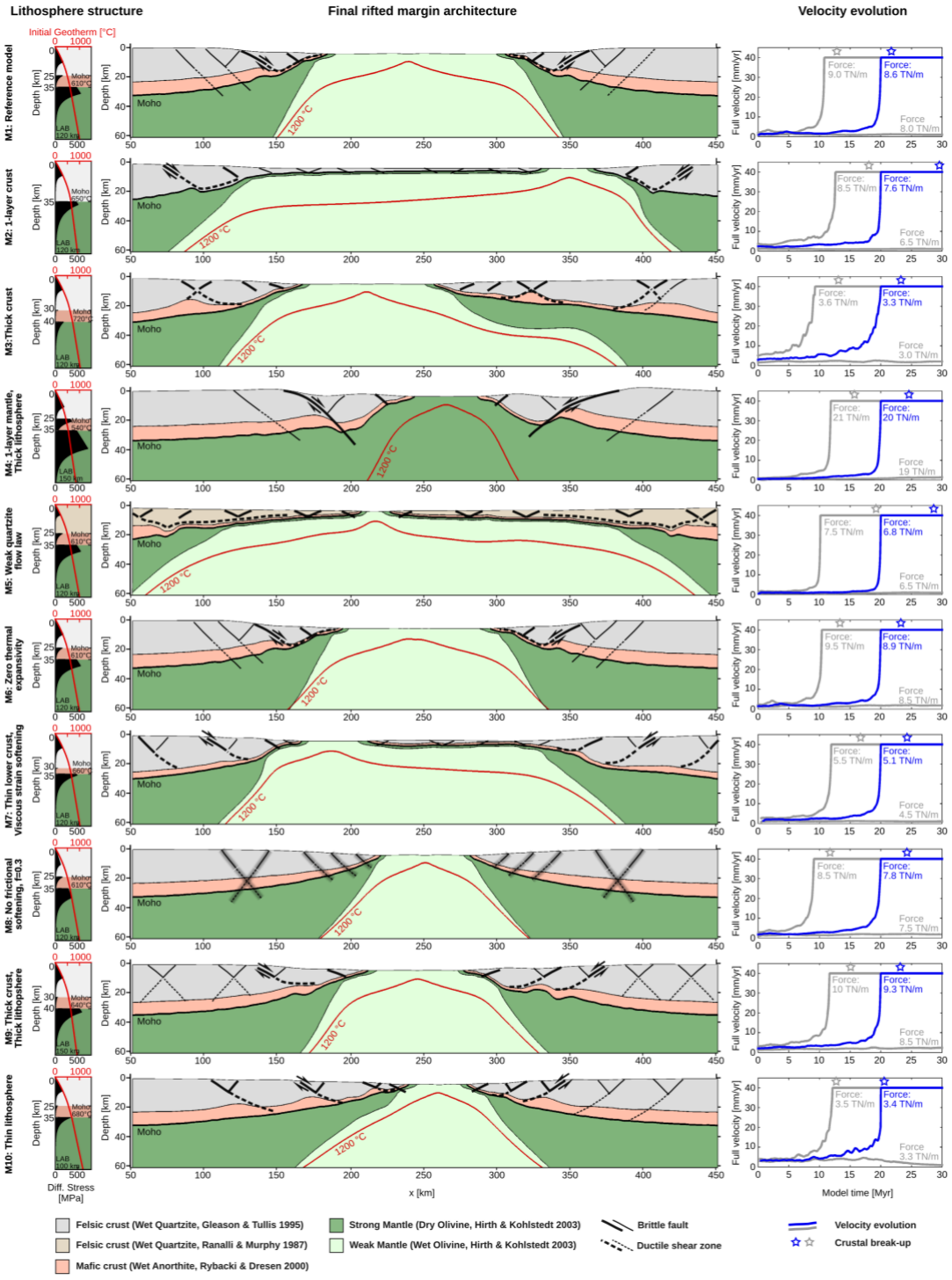

Extended Data Figure 7 | Final margin structures of numerical experiments. *Using model M1 as our reference model, we vary layer thickness, rheological flow laws, the thermal configuration, frictional softening, and thermal expansivity in order to compute models M2-M10. M5 uses the comparatively weak quartzite flow law of Ranalli and Murphy (1987)[71]. The final margin structures feature a wide range of rifted margin geometries reproducing all observed configurations of wide, narrow, symmetric and asymmetric margins. Depending on rheological evolution, extension is accommodated by brittle faults, ductile shear zones or both. For all cases, the associated time-dependent extension velocity (shown on the right in blue) exhibits the characteristic two-phase behaviour of slow rifting during the first rift phase, speed-up during lithospheric necking and fast rifting prior to break-up. Blue lines correspond to the final margin structures on the left and represent model runs where the boundary force coincides with the integrated strength of the yield strength profiles. Grey lines depict parameter variations where*

the boundary force is larger or smaller than the lithospheric strength resulting in two-phase velocities with an earlier speed-up, or decreasing rift activity reproducing failed rifts, respectively.

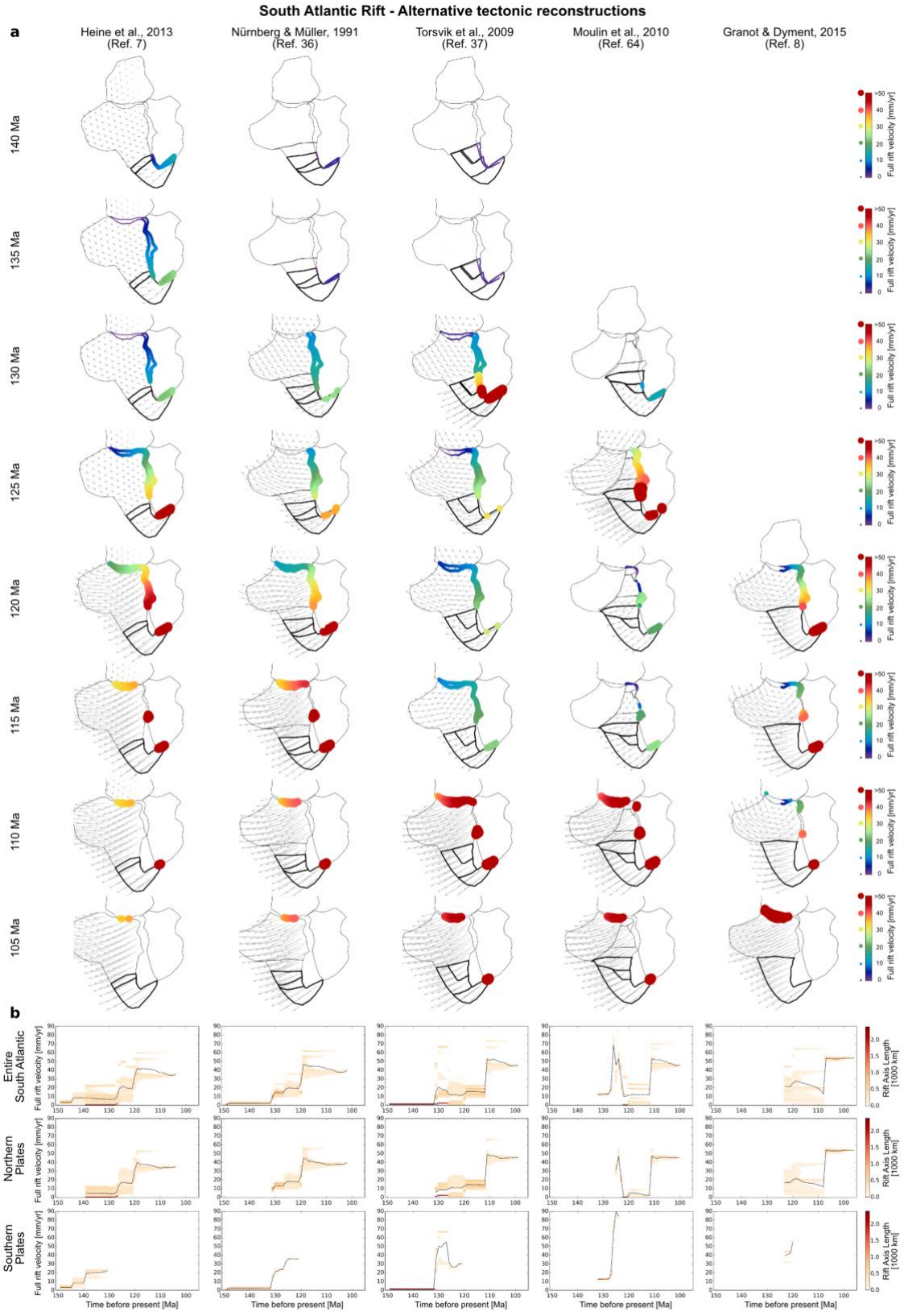

Extended Data Figure 8 | Alternative South Atlantic plate tectonic reconstructions[7,8,36,37,64]***.*** *Several end-member models are shown that differ in terms of the timing of final South Atlantic break-up, and intra-plate deformation.* ***(a)*** *Map view evolution.* ***(b)*** *Frequency of extension velocity considering the entire South Atlantic (upper panel) or only the Northern and Southern Plates (middle and lowermost panel, respectively). Southern plates are depicted as bold polygons in the map view (a). Plate models*[7,36] *with a final break-up at ~110 Myr ago depict a speed-up at 125-120 Myr ago, while models with a later break-up*[8,37,64] *at ~100*

Myr ago also involve a later rift acceleration at ~110 Myr ago. Reconstructions where large intra-plate deformation[36,37,64] decouples northern and southern South America display first a speed-up of southern South America followed by a distinct speed-up of northern South America. Plate models with less internal deformation (e.g. Heine et al., 2013) exhibit a minor acceleration of the southern plates followed by a large acceleration of entire South America. In all cases, plate kinematics show major speed-up about 10 Myr prior to break-up of the controlling rift segment.

Parameter	Units	Upper Crust		Lower Crust	Strong Mantle	Weak Mantle
Density	kg m^{-3}	2700		2850	3280	3300
Thermal expansivity	10^{-5} K^{-1}	2.7		2.7	3.0	3.0
Bulk modulus	GPa	55		63	122	122
Shear modulus	GPa	36		40	74	74
Heat capacity	J $kg^{-1}K^{-1}$	1200		1200	1200	1200
Heat conductivity	W $K^{-1}m^{-1}$	2.5		2.5	3.3	3.3
Radiogenic heat production	µW m^{-3}	1.5		0.2	0.0	0.0
Initial friction coefficient*	-	0.5		0.5	0.5	0.5
Cohesion	MPa	5.0		5.0	5.0	5.0
Rheology		Wet Quartzite	Wet Quartzite	Wet Anorthite	Dry Olivine	Wet Olivine
Flow law reference		66	71	67	68	68
Pre-exponential constant for diffusion creep	$Pa^{-1}s^{-1}$	-	-	-	2.25e-09	1.5e-09
Activation energy for diffusion creep	kJ/mol	-	-	-	375	335
Activation volume for diffusion creep	cm^{-3}/mol	-	-	-	6	4
Pre-exponential constant for dislocation creep	$Pa^{-n}s^{-1}$	8.57e-28	1.54e-17	1.79e-15	6.51e-16	2.12e-15
Power law exponent for dislocation creep	-	4.0	2.3	3.0	3.5	3.5
Activation energy for dislocation creep	kJ/mol	223	154	356	530	480
Activation volume for dislocation creep	cm^{-3}/mol	0	0	0	13	11

Extended Data Table 1 | Thermo-mechanical reference parameters. *These listed parameters are used unless indicated otherwise. *During frictional strain softening, the friction coefficient reduces linearly from 0.5 to 0.05 for brittle strain between 0 and 1. For strains larger than 1, it remains constant at 0.05.*